Desalination and Water Treatment
www.deswater.com

doi: 10.1080/19443994.2015.1085448

57 (2016) 17494–17511
August

Taylor & Francis
Taylor & Francis Group

Evaluation of the mesoporous silica material MCM-41 for competitive adsorption of Basic Violet 5BN and Basic Green from industrial dye wastewater

Meili Zhang[a], Yunhai Wu[a,b,*], Yiang Fan[b], Wenjie Zhu[b], Huaiyang Zhao[b], Aynigar Arkin[b]

[a]*Key Laboratory of Integrated Regulation and Resources Development of Shallow Lakes, Ministry of Education, Hohai University, Xikang Road, Nanjing 210098, China, Tel. +86 15240235775; email: zhangml0202@hotmail.com (M. Zhang), Tel. +86 13951770218; email: smilehhu@sina.com (Y. Wu)*

[b]*College of Environment, Hohai University, Xikang Road, Nanjing 210098, China, Tel. +86 15151826003, email: hhu_fya@163.com (Y. Fan), Tel. +86 15240246928; email: 990588357@qq.com (W. Zhu), Tel. +86 15062941220; email: 924645326@qq.com (H. Zhao), Tel. +86 13515119297; email: 626072898@qq.com (A. Arkin)*

Received 20 January 2015; Accepted 15 August 2015

ABSTRACT

MCM-41 is demonstrated to be an efficient adsorbent for the removal of two representative cationic dyes, namely Basic Violet 5BN (BV) and Basic Green (BG). Characterization of the adsorbent was studied by FTIR, X-ray diffraction, and Brunauer-Emmett-Teller. And various parameters including the solution pH, adsorbent dosage, contact time, initial cationic dye concentration, and temperature were systematically analyzed. It was found that the adsorption was pH independent and the maximum removal percentage of 86.81% BV occurred at pH 5.0 and 25°C using 0.3-g MCM-41, whereas 94.79% BG under the same experimental conditions. Besides, both the adsorptive removal of BV and BG by MCM-41 increased with the adsorbent dosage and contact time, but decreased with the initial dye concentration and temperature. In single component systems, equilibrium data were well presented by the Langmuir isotherm, suggesting the adsorption to be monolayer. And the E values (<8 kJ/mol) resulted from the D–R isotherm fitting showed the adsorption was physical in nature. The adsorption kinetics fitted better with the Lagergren pseudo-second-order model, and rate-controlling steps were both the external diffusion and intraparticle diffusion. Thermodynamic parameters (ΔG°, ΔH°, and $\Delta S^\circ < 0$) indicated that the adsorption process was feasible, spontaneous, and exothermic. Furthermore, competitive adsorption existed between the mixed dyes, and the removal efficiency and adsorption capacity of the dyes in binary component systems were lower than those in single systems. The adsorption isotherm and kinetic data of the binary component systems could also be well described by the Langmuir and Lagergren pseudo-second-order models. High recovery percentage of BV and BG by 0.1-M NaOH solution allowed excellent desorption and regeneration of the cationic dyes in practical applications.

Keywords: Competitive adsorption; Equilibrium isotherms; Kinetics; Desorption; Basic Violet 5BN; Basic Green

*Corresponding author.

1. Introduction

Numerous synthetic dyes, which are mainly discharged from various industries, such as paper, textiles, plastics, leather, food plants, and so on, are serious important sources for the water pollution due to their toxicity, carcinogenicity, high stability, and complex aromatic structures [1–4]. The widespread occurrence of dye contamination in the environment, especially in aquatic matrices has gained considerable public concerns because of the huge potential risks of disturbing the aquatic ecosystem, food chains, and even damaging human organs [5–7]. Dyes can be classified into three types, namely cationic, anionic, and nonionic based on the different ionic charge of dye molecules, among which the cationic dyes are far more noxious than anionic dyes [5,8,9]. As a consequence, the cationic dye effluents should be properly treated before being discharged into water bodies, which is of great importance [10].

A growing interest has been concentrated on methods that are highly effective, low cost, and environmental friendly, of removing cationic dyes from the industry effluents. A large number of investigations on diverse physical, chemical, and biological methodologies for treating dye-containing wastewaters have been widely conducted, such as chemical coagulation, flocculation, oxidation, ion exchange, irradiation, filtration, sedimentation, solvent extraction, reverse osmosis, electrolysis, and adsorption [1,11–14]. For the examined applications mentioned above, it was found that the adsorption technique might be a successful alternative one to control dye pollution in terms of its high efficiency, low cost, easy operation, simple design, flexible management, and minimum sludge production [1,12,15,16].

Numerous studies have been devoted to searching for suitable adsorbents [17], among which activated carbon appears to be the most commonly used for the removal of dyes/organics on account of its large adsorption capacity and surface area [18,19]. However, some disadvantages such as the relatively high cost and difficult regeneration of the activated carbon hinder its application in dye wastewater treatment, which demands for other adsorbents which are more economically viable and environmentally friendly [20].

A large amount of researches on the characterizations, and applications of the ordered mesoporous molecular sieves have been developed explosively recently [21–23]. As one of these materials, MCM-41 molecular sieves, which were a kind of novel mesoporous zeolite, synthesized by Mobil researchers in 1992 [24], have attracted abundant and still rising attention due to their distinguished properties including the large Brunauer-Emmett-Teller (BET) surface area, high pore volume, hydrophobic surface nature as well as parallel and ideally shaped pore structures without the complications of a network [25], which make it ideal for testing a lot of various existing adsorption and diffusion models [12,26,27]. In addition, MCM-41 manifests excellent performances for chemical separations and reactions of large molecular contaminants (such as dye adsorption) [22,25,28].

In the last few years, quite a lot of different kinds of adsorbents have been used to remove dye molecules in single component systems. However, most of the industrial effluents discharged contain more than one type of dye contaminants, making it great and practically important to investigate the influences of multi-solute systems on the adsorption performance [29].

Thus the present study was devoted to investigating the adsorption behavior of MCM-41 to remove two representative cationic dyes, Basic Violet 5BN (BV) and Basic Green (BG). The effects of solution pH, adsorbent dosage, contact time, initial dye concentration, and temperature were studied. The equilibrium, kinetic data, and thermodynamic parameters of single component systems were processed to understand the adsorption mechanism of BV and BG onto MCM-41. Furthermore, isotherms and kinetics of the binary component systems were analyzed in comparison with the single systems. Desorption experiments were carried out to test the regeneration of MCM-41 which would help lay a theoretic foundation of more practical and economical applications.

2. Materials and methods

2.1. Reagents

Two basic cationic dyes (BV and BG) were selected as the targeted adsorbates, which were applied as commercial salts without further purification. The two dyes molecular characteristics and structures were illustrated in Fig. 1. Different aqueous solutions of the dyes were prepared by dissolving them in distilled water. A Shimadzu UV-1201 Spectrophotometer and the corresponding calibration curves were adopted to determine the residual concentrations of each dye in the mixture solutions. At least three runs were conducted for each sample and the average value was recorded. In addition, all compounds used in this work were of analytical grade. All glassware were cleaned several times and rinsed with distilled water.

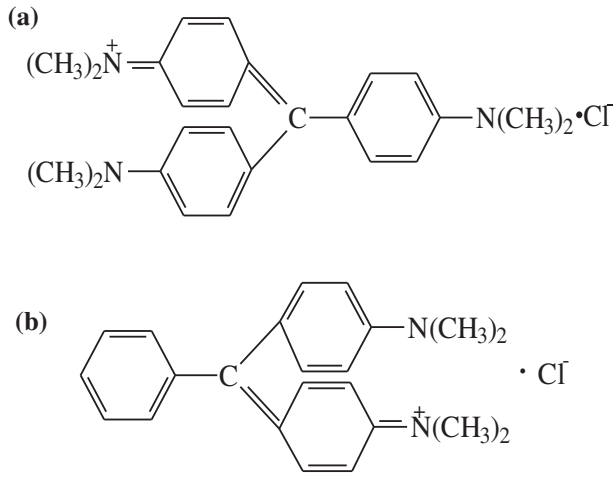

Fig. 1. Chemical structures and general characteristics of BV and BG. (a) BV, molecular formula: $C_{25}H_{30}N_3Cl$, molecular weight (g mol^{-1}): 408.03, λ_{max} (mm): 584 and (b) BG, molecular formula: $C_{23}H_{25}N_2Cl$, molecular weight (g mol^{-1}): 364.90, λ_{max} (mm): 618.

2.2. Preparation and characterization of the adsorbents

The preparation method of mesoporous MCM-41 was on the basis of the previous literature [22,30]. The MCM-41 powder was crystallized from an alkaline solution containing cetyltrimethylammonium bromide (CTABr, 99%, Merck), sodium silicate solution (Na_2O, 7.5–8.5%, SiO_2, 25.8–28.5%, Merck), sulfuric acid (98%, Merck), and distilled water in the mole ratio of 1 CTABr: 1.76 Na_2O: 6.14 SiO_2: 335.23 H_2O: 1.07 H_2SO_4. After 24 h of crystallization at room temperature, the MCM-41 powder was filtered, washed, and dried before it was calcined in a furnace at 450°C for 4 h for removing the organic template.

The obtained MCM-41 adsorbent was characterized using different methods. Fourier Transform Infrared Spectroscopy (FTIR, JASCO 5300) was employed to observe qualitative identification of functional groups on the surface of the adsorbent, the spectra of which were within the range of 500–4,000 cm^{-1} wavenumber. Besides, powder X-ray diffraction (XRD) measurements for the adsorbent before and after adsorption were performed with an X-ray diffractometer (ARL Corporation, Switzerland) instrument using Cu $K\alpha$ radiation at 40 kV and 40 mA in the 2θ range 0–90°. The point of zero charge (PZC) of MCM-41 was determined by the solid addition method [31]. Nine vials containing solutions with different pH values (2.0–10.0) and 0.10-g MCM-41 were shaken for 24 h at room temperature, and the final pH was determined. The Quantachrome Autosorb-I Physical Model was applied to determine the Brunauer-Emmett-Teller (BET, MICROMERITICS, ASAP 2010, USA) surface area, total pore volume and mean pore radius.

2.3. Adsorption experiments

The effect of pH was investigated by adding 0.3-g MCM-41, respectively, into two 250-mL flasks containing 100-mL BV and BG severally, both the concentrations of the dye aqueous solutions were 100 mg/L. The solution pH was adjusted with 0.1-M HCl or 0.1-M NaOH solutions to the range of 2.0–10.0. Then the tightly stopped flasks were put on temperature-controlled shaker at 180 rpm and 25°C for 4 h. Then samples were collected, filtered, and measured.

The impact of adsorbent dosage on adsorption, at the optimum pH 5.0, was determined by adding adsorbent in the range of 0.05–0.5 g. After being agitated on a shaker at 180 rpm and 25°C for 4 h, samples were filtered and analyzed.

Moreover, samples collected at 30, 60, 120, 180, 240, and 300 min, respectively, were measured so as to explore the influence of contact time on adsorption. And the effect of the initial dye dosage was conducted by diluting each dye solution of 300 mg/L into 20, 50, 100, 150, 200, and 250 mg/L separately.

For the binary component systems, experiments were conducted at the conditions of 25°C, pH 5.0, and MCM-41 dosage 0.3 g. As to the adsorption isotherms, initial concentrations of the dyes were within the range of 100–300 mg/L, and samples were filtered and measured after 4 h. And for the kinetic study, the initial concentration and volume of both the two dyes were, respectively, 100 mg/L and 50 mL, and samples were collected and analyzed at 30, 60, 120, 180, 240, 300, and 360 min in sequence.

In addition, for the desorption study, firstly, 0.3-g MCM-41 was added into each single component solution with the dye concentration of 100 mg/L. After adjusting pH to 5.0, the samples were put on temperature-controlled shaker at 180 rpm and 25°C for 4 h. Then the saturated MCM-41 was collected, filtered, washed with distilled water, dried, and kept in contact with 100 mL of three different desorbing solutions: 0.1 M NaOH, 0.1 M NaOH, and 10% C_2H_5OH, respectively. The mixtures were shaken in a temperature-controlled rotary shaker at 25°C and 180 rpm for 12 h, and then filtered and measured.

The adsorptive removal efficiency (η) was determined according to the following equation:

$$\eta = \frac{C_0 - C_e}{C_0} \times 100\% \quad (1)$$

Dyes uptake (q_e) was calculated through the equation as below:

$$q_e = \frac{(C_0 - C_e)}{M} V \quad (2)$$

The desorption efficiency (γ) was determined according to the equation below:

$$\gamma = \frac{C_2 \times V_2}{(C_0 - C_e) \times V_1} \times 100\% \quad (3)$$

3. Results and discussion

3.1. Characterization of the adsorbent before and after the adsorption processes

The qualitative identification of functional groups on the surface of the synthesized MCM-41 before and after adsorption of BV and BG were observed by FTIR spectroscopic analysis, as illustrated in Fig. 2. Broad and strong bands (3,250–3,750 cm^{-1}) with peaks appeared at around 3,400 cm^{-1}, probably owing to the asymmetric stretching mode of the adsorbed H_2O molecules and O–H bonds [32]. The peaks at 1,635 cm^{-1} were attributed to bending vibrations of the adsorbed water molecules. Three well-known vibrational modes of a–SiO_2 are visible in all spectra [33]. The symmetric and asymmetric stretching vibrations of Si–O–Si groups were observed around 793 and 1,078 cm^{-1}, respectively. And the bending vibration mode of Si–O–Si could be seen at around 500 cm^{-1}. After the adsorption of BV and BG onto MCM-41, the infrared spectrum showed no apparent change except a fluctuation within the range of 1,280–1,470 cm^{-1}, which could be ascribed to C–H deformation vibrations. The spectral features resemble those reported by previous researchers [33,34].

The small angle XRD patterns accompanied with the adsorption processes of BV and BG dyes onto MCM-41 were illustrated in Fig. 3. The presence of both (100) and (200) diffraction peaks in the primary/synthesized MCM-41 are the evidence of good crystallinity of the prepared powder. It could be clearly observed that MCM-41-BV and MCM-41-BG become less crystalline than the prepared MCM-41, which was indicated by the sharp decrease in the intensity of most MCM-41 peaks [36]. Besides, for both MCM-41-BV and MCM-41-BG, the collapse is further confirmed with the disappearance of (100) and (110) peaks of the original MCM-41 material. However, the changes in the porous structures of MCM-41-BV and MCM-41-BG were more likely due to the inherent disorder induced by the adsorption of BV and BG because of the existence of the main peak signal of the XRD pattern of MCM-41 [33].

The point of zero charge (pH_{PZC}) can be an excellent parameter for the description of the interaction at the solid/solution interfaces [22]. As stated by [31], cationic adsorption is favored when the solution pH is higher than pH_{PZC}. In the present work, the pH_{PZC} value is found to be 3.8, lower than the optimum solution pH 5.0, indicating the negatively charged surface of the adsorbent MCM-41, which further supports the

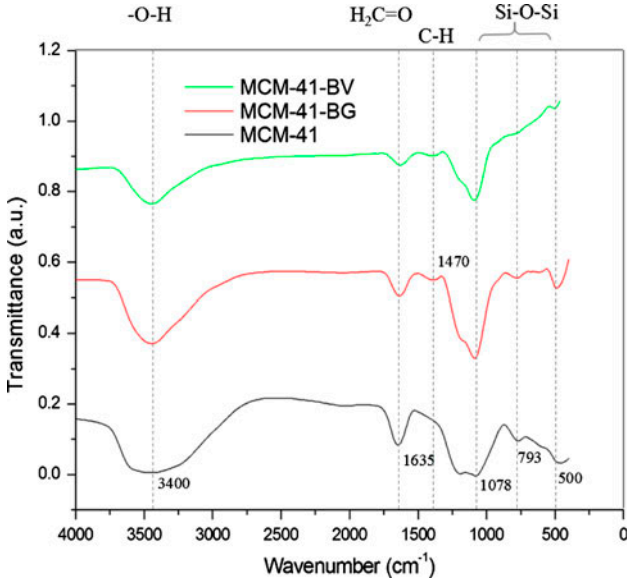

Fig. 2. FTIR spectra of MCM-41, MCM-41-BV and MCM-41-BG.

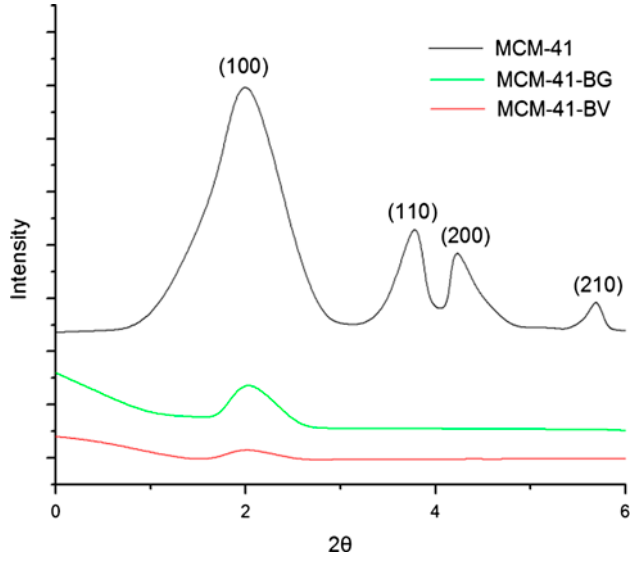

Fig. 3. The small angle XRD patterns of MCM-41, MCM-41-BG, and MCM-41-BV.

electrostatic interaction between the cationic dyes and the adsorbent MCM-41 during the adsorption process.

As determined from the nitrogen adsorption-desorption isotherms measured by the Quantachrome Autosorb-I Physical Adsorption Model at −195℃, the synthesized MCM-41 with the BET surface area (921 m^2/g), total pore volume (0.94 cm^3/g), and mean pore radius (3.02 nm) is the typical value of surfactant-assembled mesostructures [35].

3.2. Adsorption in single component systems

3.2.1. Effect of solution pH

The effect of solution pH on the adsorption of BV and BG using MCM-41 was studied in the pH range of 2.0–10.0 which is shown in Fig. 4. It was found that the removal efficiency and adsorption capacity of BV and BG tended to decrease obviously at low and high pH. The adsorptive removal percentage of BV (BG) increased from 66.62 (69.33) to 86.81% (94.79%) due to the rise in pH from 2.0 to 5.0, while dropped to 84.01% (73.69%) as pH continued to reach 10.0. The maximum dye adsorption occurred at pH 5.0.

Electrostatic attraction exists between the negatively charged surface of the adsorbent MCM-41 and positively charged cationic BV and BG dye molecules at pH 2.0–10.0, which leads to a relatively good adsorption performance. However, under the conditions of low and high pH, the obvious decreasing removal efficiency of dyes could be also explained by the reducing of MCM-41 structure stability. In addition, low pH resulted in a considerable amount of H^+ ions in the aqueous solution. On one hand, neutralization occurred between the hydroxy groups (−OH) on MCM-41 and H^+ ions in the solution, which could lower the charge of the adsorbent surface. On the other hand, more H^+ ions would take part in competing for the available adsorption sites with the cationic dyes in the system [36]. The dissociation of the cationic dye molecules and their combination with the adsorbent MCM-41 in the aqueous solution are illustrated in Fig. 5.

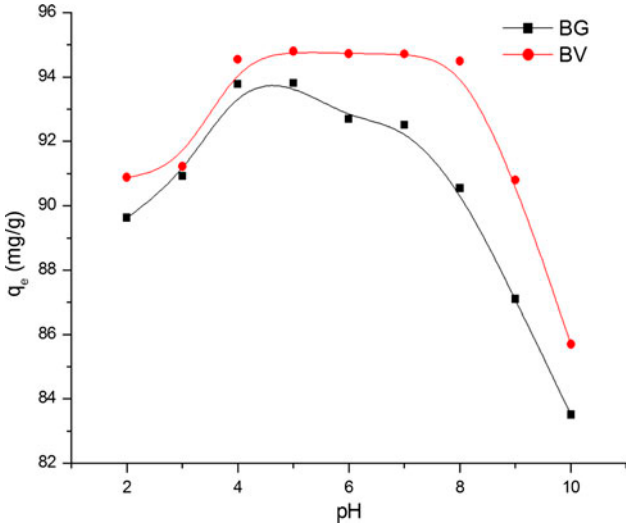

Fig. 4. Effect of solution pH on adsorption of BV and BG in single component systems (Conditions: 25℃, dye concentration 100 mg/L, MCM-41 dosage 0.3 g).

3.2.2. Effect of adsorbent dosage

As seen from Fig. 6, the increasing adsorbent MCM-41 dosage resulted in increase of the adsorptive removal ratios, which is in consistent with our research of anionic dye adsorption [37]. It was found that both the removal ratios of BV and BG increased quickly and eventually reached to more than 86.00% as the MCM-41 dosage increased from 0.05 to 0.3 g, and afterward, the removal ratios tended to become sluggish in spite of the continuous adding of MCM-41. Therefore, 0.3 g was chosen as the optimal adsorbent dosage in this work.

As more adsorbent dosage brought about more contacting surface area and more available adsorption sites, more dye molecules were adsorbed by the adsorbent hence causing the increase in adsorptive removal ratios. Whereas drop of the amount of adsorbed dyes might be due to that some adsorption active sites had not reached the state of saturation [38]. Another explanation was because of the spilt in the flux or the concentration gradient between the solute concentration in the solution and the solute concentration on the surface of the adsorbent. Consequently, the amount of dye adsorbed onto unit weight of adsorbent dropped with the rising adsorbent dosage, resulting in decrease of the q_e values [20,39,40].

3.2.3. Effect of contact time

The effect of contact time on the adsorption of BV and BG onto MCM-41 was investigated and results are presented in Fig. 7. It was found that the equilibrium capacity of adsorption and removal ratios of BV and BG increased continually with time during the first 240 min, and then the adsorption rate became gradually constant, which indicated the establishment of dynamic equilibrium state. At the point of 240 min, the adsorptive removal ratios of BV and BG were 86.17 and 93.95%, respectively, and no obvious increase afterward, demonstrating that the equilibrium

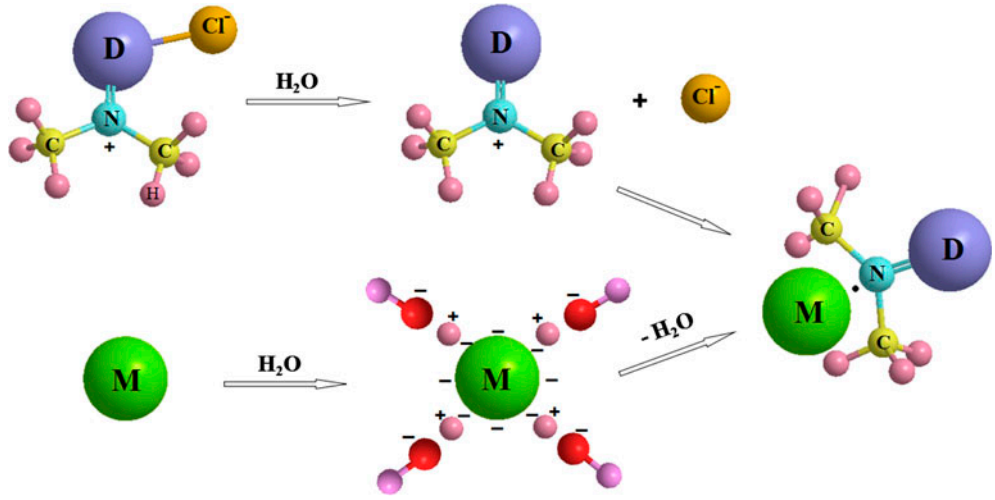

Fig. 5. Schematic illustration of the adsorption reactions in aqueous solutions. D: the remaining fractions of the two cationic dye molecules (for BV, the molecular formula of the remaining fraction is $C_{23}H_{24}N_2$, and for BG, the molecular formula of the remaining part is $C_{21}H_{19}N$, both of whose molecular structures can be seen from Fig. 1). M: MCM-41.

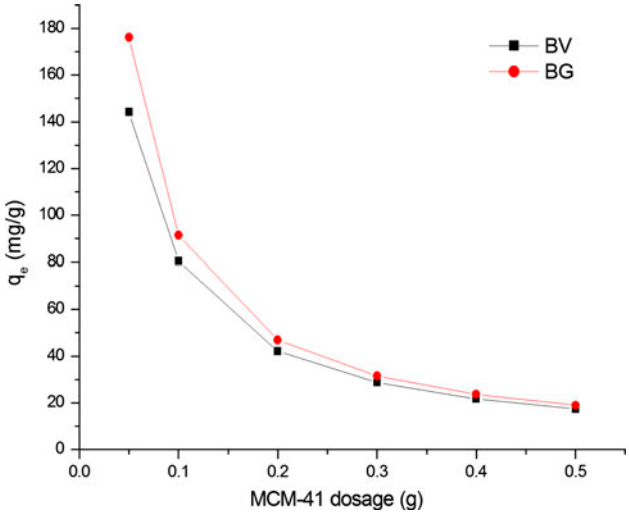

Fig. 6. Effect of adsorbent MCM-41 dosage on adsorption of BV and BG in single component systems (Conditions: pH 5.0, 25℃, dye concentration 100 mg/L).

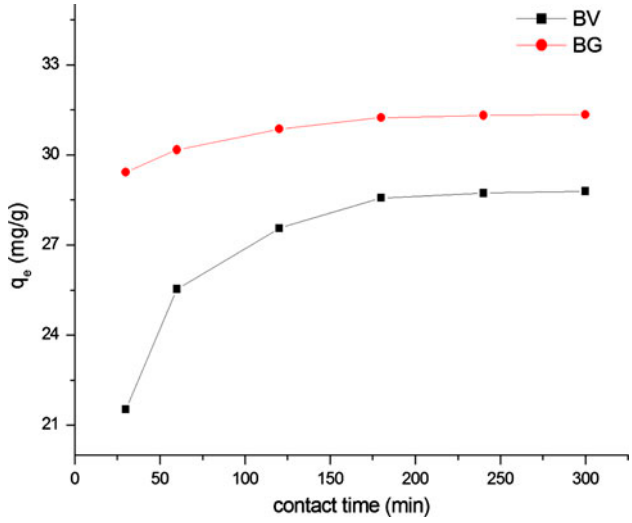

Fig. 7. Effect of contact time on adsorption of BV and BG in single component systems (Conditions: pH 5.0, 25℃, dye concentration 100 mg/L, MCM-41 dosage 0.3 g).

time of the adsorption of BV and BG onto MCM-41 was approximately 240 min.

The reason for this observation is thought to be the fact that, the interaction and affinity between the negatively charged adsorbent and positively charged dyes were enhanced, simultaneously the resistance to the uptake of dyes diminished as the mass transfer driving force increased in the early stage, which led to a rapid initial adsorption phase. After that, a progressive decline of the adsorption rate occurred, which might be ascribed to the gradually decreasing diffusion rate of BV and BG dye molecules penetrating into the pores of the adsorbent MCM-41 [41].

3.2.4. Effect of initial cationic dye concentration

The influence of initial dye concentration on the adsorption performance was illustrated in Fig. 8. As seen from Fig. 8, the adsorption capacity of BV (BG) at equilibrium state increased from 6.11 (6.51) to 66.73 mg/g (78.33 mg/g), whereas the adsorptive removal percentage of BV (BG) decreased from 91.63

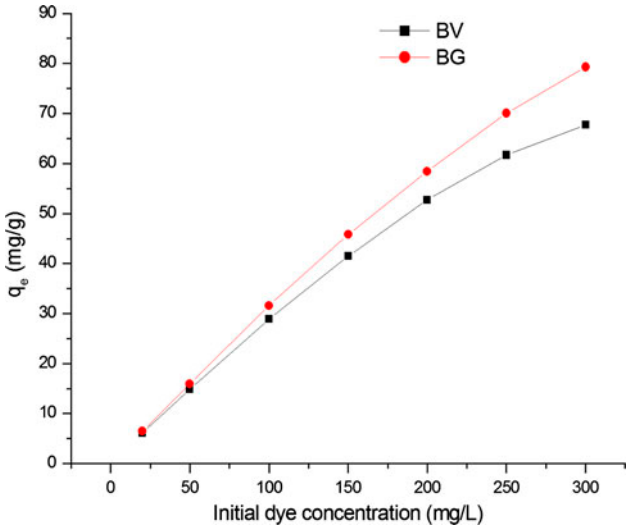

Fig. 8. Effect of initial dye concentration on adsorption of BV and BG in single component systems (Conditions: pH 5.0, 25℃, MCM-41 dosage 0.3 g).

(97.79) to 67.53% (79.33%) as the initial concentrations of BV and BG increased from 20 to 300 mg/L.

Firstly, the increase in adsorption capacity with the rising initial dye concentration might be attributed to that, on one hand, more amount of adsorbates in the aqueous solution aggrandized the number of adsorbates that took part in the competition for available active adsorption sites on the surface of adsorbent; on the other hand, higher concentration of dye molecules could strengthen the collision frequency between the dyes and adsorbent [42,43]. Additionally, the available adsorption sites were reduced due to the continuous accumulation of BV and BG dye molecules in the vacant active sites of adsorbent whose quantity was limited, thus resulting in the steadily declining of the adsorption rates of the two cationic dyes onto MCM-41 [44].

3.2.5. Adsorption equilibrium isotherms

The distribution of cationic dyes between the liquid phase and the adsorbent at the state of equilibrium is obviously of great importance to establish, which can be generally described through several isotherm models [36]. For the present study, the Langmuir, Freundlich, Temkin, and Dubinin-Radushkevich (D–R) models were adopted to measure the distribution coefficient during the adsorption processes at different temperatures, whose equations are listed in Table 1.

The adsorption equilibrium is very vital for describing the interaction between the adsorbent and the adsorbate molecules as well as the relationship between the adsorption capacity q_e (mg/g) and the liquid phase dye concentration at equilibrium C_e (mg/L) [45]. The Langmuir isotherm is effective for adsorption of the adsorbate molecules in the aqueous solution as monolayer adsorption onto the adsorbent surface which contains a finite amount of active adsorption sites [46]. Besides, the K_F and n values are two Freundlich constants corresponding to the adsorption capacity and the adsorption intensity, respectively. Higher value of K_F demonstrated higher affinity and higher adsorption capacity, and higher n value indicated that it is easier for the adsorbate to be taken up by the adsorbent [47]. The Freundlich isotherm model is much valid for multilayer adsorption, which was originated from the assumption of the heterogeneous surface with the interaction between the adsorbate molecules as well as a nonuniform distribution of adsorption heat on the adsorbent surface [20,46]. The value of K_L is indicative of the adsorption of the adsorption capacity of the adsorbent [20]. The Temkin isotherm model takes the impact of the indirect interactions of the adsorbate molecules on isotherms into consideration by suggesting the linear fall in the heat of all the adsorbate adsorption with the coverage of the solute and the adsorbent interactions on the surface of the adsorbent [14,31]. The Temkin constants K_T and b can be calculated from the plot of q_e*vs.* ln C_e. D–R model is valid for the determination of nature of the adsorption process as either chemical or physical, which is judged by the mean free energy of adsorption E (more than 8 kJ/mol or not) [48].

In this work, the adsorption equilibrium isotherm data of BV and BG onto the adsorbent MCM-41 were analyzed with four models, namely the Langmuir, Freundlich, Temkin, and D–R isotherm models. In addition, the four isotherm parameters were listed on Table 2. R^2 values are used to determine the optimum isotherm for describing the adsorption process [16,49]. The Langmuir isotherm model gave the best fit than Langmuir and D–R models as shown by the highest R^2 value as seen in Fig. 9, indicating it the monolayer adsorption of the BV and BG dyes onto the adsorbent. Similar results have been reported for the adsorption of basic dyes by MCM-41 [22]. Table 2 shows that the adsorption capacity of BV and BG onto MCM-41 decreased with the rising temperature, suggesting that high temperature might not favor the adsorption process. All the n values of the Freundlich isotherm model are more than 1.0 at all temperatures, indicative of high adsorption intensity and favorable nature of the adsorption processes [50]. The low R^2 values of the Temkin model show its inapplicability for interpretation of experimental data [51]. What is more, all

Table 1
Summary of the isotherm and kinetic models applied in the present work

Models	Mathematical equations	Serial number	Refs.
Isotherm models			
Langmuir	$\frac{C_e}{q_e} = \frac{1}{q_m K_L} + \frac{C_e}{q_m}$	(4)	[14]
Freundlich	$\ln q_e = \ln K_F + \frac{1}{n} \ln C_e$	(5)	[14]
Temkin	$q_e = \frac{RT}{b} \ln K_T + \frac{RT}{b} \ln C_e$	(6)	[14]
Dubinin–Radushkevich (D–R)	$\ln q_e = \ln q_m - K\left(RT \ln\left(1 + \frac{1}{C_e}\right)\right)^2$	(7)	[14]
Kinetic models			
Pseudo-first-order	$\ln (q_e - q_t) = \ln q_e - k_1 t$	(8)	[16]
Pseudo-second-order	$\frac{t}{q_t} = \frac{1}{k_2 q_e^2} + \frac{t}{q_e}$	(9)	[16]
Spahn and Schlunder	$\ln C_t = \ln C_0 - k_{ext} t$	(10)	[52,53]
Intraparticle diffusion	$q_t = k_{p,i} t^{0.5} + C$	(11)	[16]
Elovich	$q_t = \frac{1}{\beta} \ln(\alpha\beta) + \frac{1}{\beta} \ln t$	(12)	[16]

of the E values of the D–R isotherm are less than 8 kJ/mol, suggesting that the adsorption process of BV and BG onto MCM-41 is of a physical nature [22].

3.2.6. Adsorption kinetics

Several kinetic models are available to express the controlling mechanism of the adsorption process in this work, five kinetic models: Lagergren's pseudo-first-order, pseudo-second-order, Spahn and Schlunder, intraparticle diffusion, and Elovich models were applied, which are listed together with the isotherm models in Table 1.

When selecting the adsorbent material, the adsorption rate is considered as a vital factor. Hence, in order to elucidate the adsorption rate as well as investigate the mechanism and the rate-controlling steps during the overall adsorption processes of BV and BG dye molecules onto MCM-41 [54]. Five kinetic models including the pseudo-first-order, pseudo-second-order, Spahn and Schlunder, intraparticle diffusion, and Elovich models are applied to examine the adsorption process, which are shown in Fig. 10. And the experimental parameters calculated from the kinetic model equations are given in Table 3.

Seen from Table 3, the calculated q_e values of the pseudo-first-order are not in accordance with the experimental q_e values, therefore it did not fit well. Whereas the calculated adsorption capacity values of the equilibrium state of the pseudo-second-order are in consistent with the experimental data, additionally the R^2 values are much higher compared to the pseudo-first-order kinetic model. Thus, the pseudo-first-order model could be far more applicable for the description and prediction of the adsorption kinetic data for the whole adsorption process, which suggested that the overall rate of the cationic dye adsorption controlling factor appeared to be the chemisorption [47]. Furthermore, the result also demonstrated that the adsorption processes of BV and BG dye molecules onto the adsorbent MCM-41 were likely to proceed via surface exchange reactions till the available active sites of the adsorbent surface were occupied completely; whereafter, the BV and BG molecules probably would diffuse into the inner space of the adsorbent for further interactions [55].

A good knowledge of the mass transfer mechanism of adsorption in the liquid phase is very necessary for designing the adsorption system that is both valid and cost-effective. As a result, the Spahn and Schlunder, and intraparticle diffusion models were chosen to analyze the adsorption of BV and BG onto MCM-41.

For the Spahn and Schlunder model, a good linear correlation between ln C_t and t will appear if the rate of the liquid film diffusion is predominant in the entire adsorption process. It was clearly seen from Fig. 10(c) that, a comparatively better linear relationship between ln C_t and t turned up in the initial 180 min with the higher R^2 (BV: 0.8689, BG: 0.9526), elucidating a greater influence of external diffusion on the adsorption rates of BV and BG onto MCM-41 in the first 180 min.

The mechanism of the adsorption of the adsorbates from aqueous solution by mesoporous adsorbents

Table 2
Adsorption isotherm constants for adsorption of BV and BG onto MCM-41 at various temperatures in single component systems

Dyes	Temperature (°C)	Langmuir			Freundlich			D–R				Temkin		
		q_m	K_L	R^2	K_F	n	R^2	Q_m	K	R^2	E	b	K_T	R^2
BV	25	90.1765	0.0292	0.9944	11.0843	1.9523	0.9777	42.9455	0.1533	0.7062	1.806	162.3225	2.0377	0.9494
	30	87.0851	0.0350	0.9971	8.0421	1.7047	0.9725	42.3251	0.1772	0.6953	1.680	145.5172	1.0942	0.9594
	40	85.0323	0.0404	0.9973	0.9718	0.9972	0.9999	41.8101	0.2110	0.6936	1.539	93.7076	0.1400	0.8817
BG	25	99.7308	0.0470	0.9934	5.2120	1.6582	0.9733	46.9691	0.0241	0.6643	4.555	154.0280	0.6106	0.9666
	30	94.1121	0.0674	0.9945	4.6748	1.6055	0.9745	47.1445	0.0564	0.6922	2.977	153.3610	0.5320	0.9630
	40	88.7959	0.1033	0.9859	5.2120	1.5394	0.9780	46.2269	0.0892	0.6835	2.368	154.3648	0.4506	0.9532

includes three consecutive steps as follows: (a) film diffusion or the external surface adsorption, (b) intraparticle diffusion or pore diffusion onto the adsorbent surface, and (c) final equilibrium stage or the adsorption onto the interior sites [47,54,56]. One or more than one of the three steps above can be the rate-controlling steps of the adsorption [56].

According to the intraparticle diffusion model, the plot of q_t vs. $t^{1/2}$ in Fig. 10(d) shows a double straight-line nature, suggesting that there existed two steps controlling the adsorption rate which could be the gradual adsorption phase and the equilibrium phase. On condition that the plot of q_t and $t^{1/2}$ is in a good linear relationship and the linear does pass through the origin, the intraparticle diffusion could be considered as the only step controlling the adsorption rate [57]. From Fig. 10(d), it can be seen that, despite that good linear relationships were revealed, the lines do not go through the point of origin, demonstrating that the intraparticle diffusion is not the only adsorption rate-controlling step in the whole adsorption process and a few other options could be drawn into the process [58]. Moreover, during the second period of the gradual adsorption, the adsorption rates become slower and slower, which might be ascribed to the quite low concentration of the residual cationic dye molecules in the aqueous solution [59]. As a consequence of that the adsorption rate ($k_{p,i}$) in the second stage of the intraparticle diffusion for BV was smaller than that of BG, the removal percentage of BV by MCM-41 is correspondingly smaller than BG, which might be related to the molecular sizes of the two cationic dyes. The smaller size of BG molecules could accelerate more BG molecules to diffuse into the inner pores of MCM-41, resulting from which the adsorption capacity of BG by MCM-41 became greater [37,60,61].

For the Elovich kinetic model which is often successfully applied to describe the second-order kinetic assuming that the actual solid surfaces are energetically heterogeneous [4,62], the initial adsorption rate α and the desorption constant β were calculated from the intercept and the slope of the straight line, by plotting q_t*vs.* $\ln t$ at three different temperature (25, 30, and 40°C). The R^2 values suggest that, the Elovich model agrees much poorer than the pseudo-second-order, which is in agreement with the previous literature [62]. Besides, it is also found that values of α and β decrease with the rising temperature for both the dye adsorption (data not shown here), supporting the conclusion that the adsorption of the basic cationic dye adsorption process onto MCM-41 is exothermic, in consistent with the result of Aljeboree et al. [63].

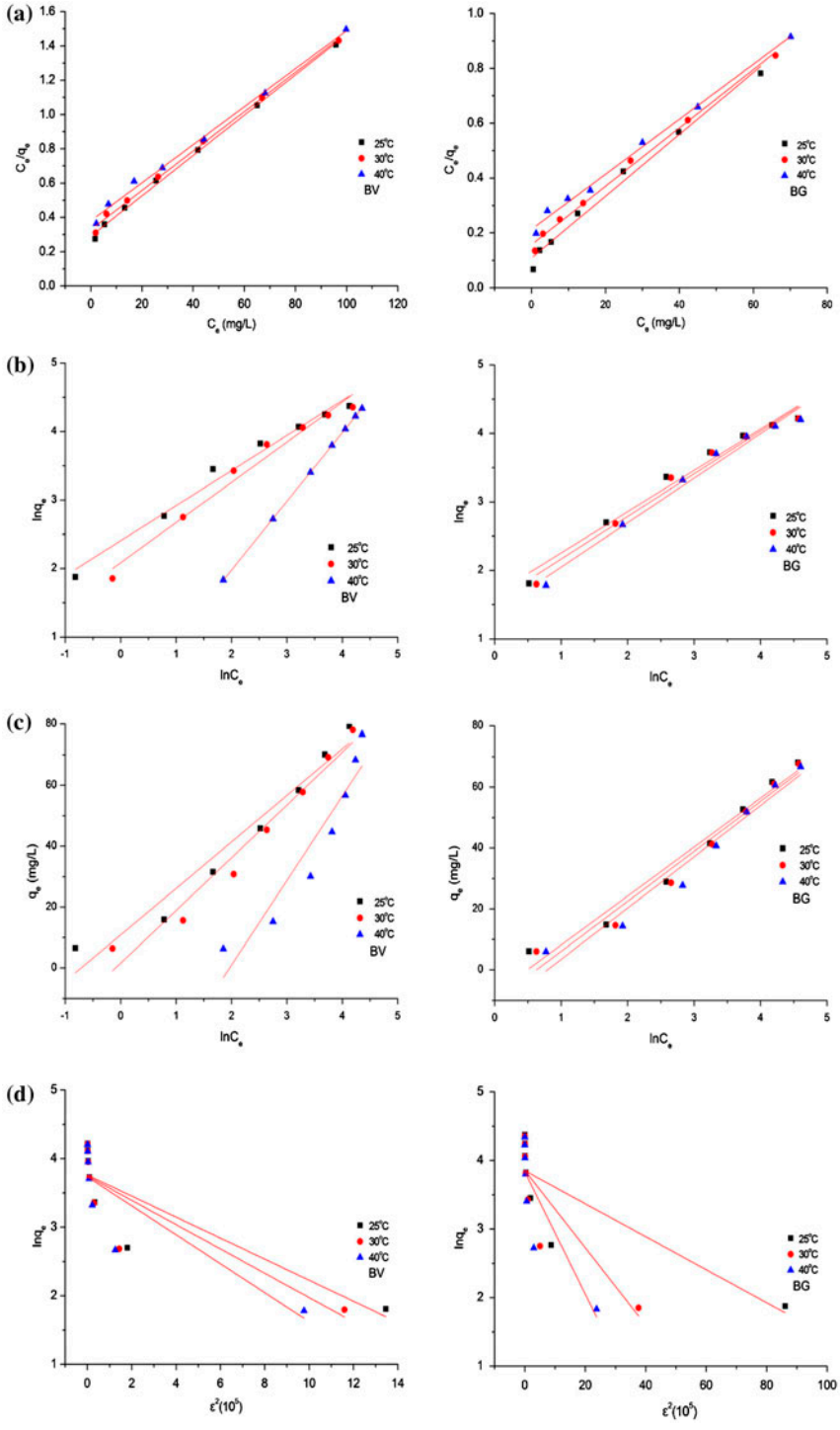

Fig. 9. Adsorption equilibrium isotherms of BV and BG onto MCM-41 in single component systems. (a) Langmuir isotherm model fitting, (b) Freundlich isotherm model fitting, (c) Temkin isotherm fitting, and (d) D–R isotherm model fitting (Conditions: pH 5.0, 25°C, MCM-41 dosage 0.3 g).

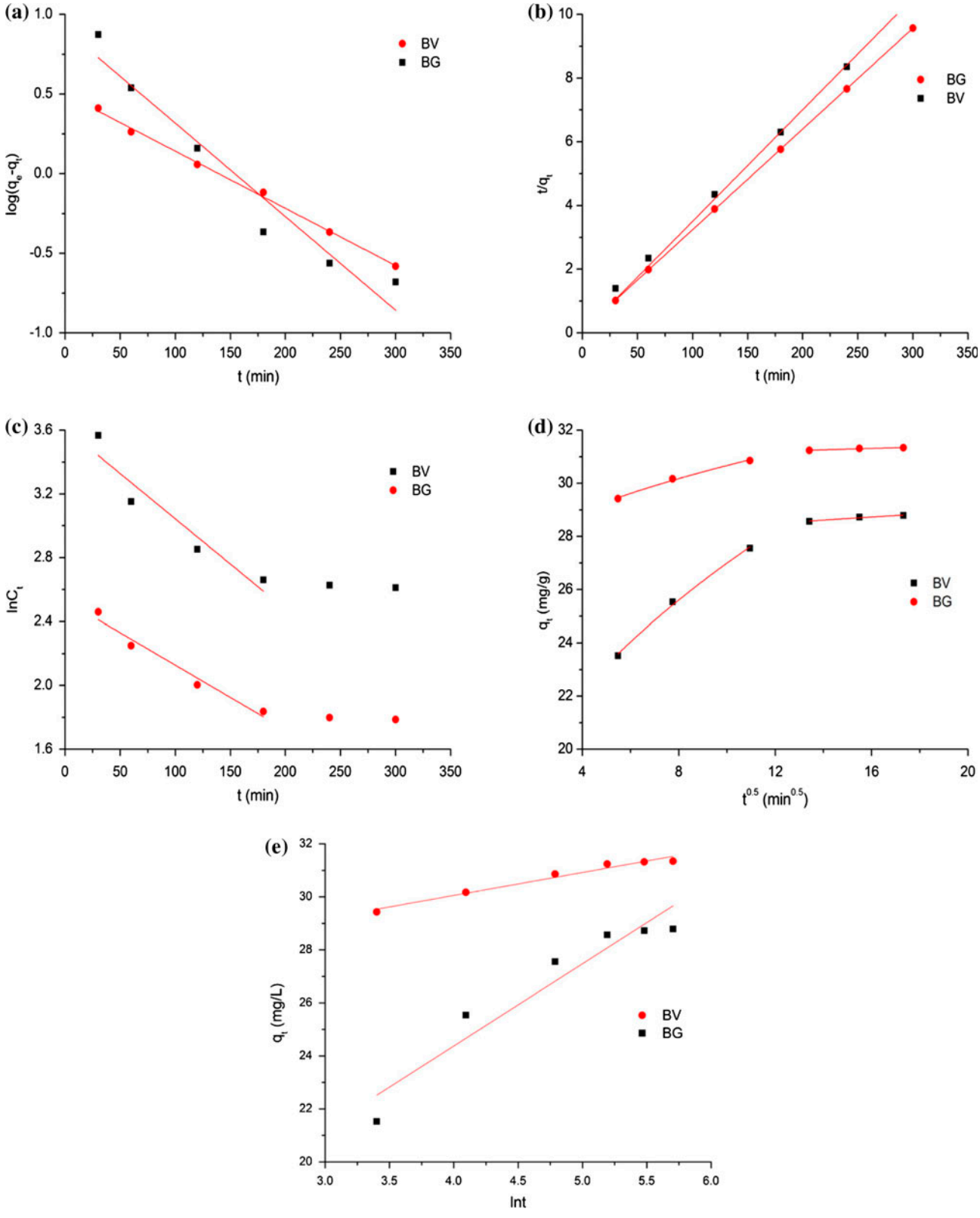

Fig. 10. Adsorption kinetics of BV and BG onto MCM-41 in single component systems. (a) Pseudo-first-order kinetic model fitting, (b) Pseudo-second-order kinetic model fitting, (c) Spahn and Schlunder model fitting, (d) Intraparticle diffusion model fitting, and (e) Elovich model fitting (Conditions: pH 5.0, 25℃, MCM-41 dosage 0.3 g).

Table 3
Kinetic parameters for adsorption of BV and BG onto MCM-41 in single component systems

Dyes	Pseudo-first-order kinetic model			Pseudo-second-order kinetic model			Spahn and schlunder model	
	k_1	q_e	R^2	k_2	q_e	R^2	k_{ext}	R^2
BV	0.0135	2.4707	0.9354	0.0560	28.5342	0.9957	0.0056	0.8689
BG	0.0082	1.6491	0.9968	0.0122	31.6306	0.9999	0.0040	0.9526

Dyes	Intraparticle diffusion model				Elovich model		
	$k_{p,2}$	R^2	$k_{p,3}$	R^2	α	β	R^2
BV	4.1474	0.9952	0.4502	0.9343	146.1085	0.3221	0.8976
BG	1.4729	0.9897	0.2087	0.8805	1.8569×10^{13}	1.1545	0.9637

3.2.7. Adsorption thermodynamics

In order to investigate the thermodynamic behavior of BV and BG adsorption by MCM-41, thermodynamic parameters such as Gibbs free energy change (ΔG°), enthalpy (ΔH°) and entropy (ΔS°) were calculated using the following equations [12]:

$$K_0 = \frac{C_{ad}}{C_e} \tag{4}$$

$$\Delta G^\circ = -RT \ln K_0 \tag{5}$$

$$\ln K_0 = \frac{\Delta S^\circ}{R} - \frac{\Delta H^\circ}{RT} \tag{6}$$

For the purpose of better estimation of the impact of various temperatures (25, 30, and 40°C in this work) on the adsorption capacity of the two cationic dyes onto MCM-41, the thermodynamic parameters including Gibbs free energy (ΔG°), enthalpy (ΔH°), and entropy (ΔS°) were analyzed. And the results were summarized in Table 4.

As known from Table 4, all values of Gibbs free energy (ΔG°), enthalpy (ΔH°), and entropy (ΔS°) are negative. The negative values of ΔG° indicated the adsorption of BV and BG onto MCM-41 is spontaneous and feasible in nature. In addition, the increase in ΔG° values with temperature rising demonstrated that the adsorption of BV and BG by MCM-41 became less favorable at higher temperature. The negative ΔH° values suggested that the adsorption process is exothermic in nature, and there is electrostatic attraction between the adsorbent and adsorbates. What is more, the negative ΔS° further confirmed the decrease in randomness at the solid-solution interface during the adsorption processes of BV and BG on the vacant active sites of the adsorbent MCM-41 [64].

3.3. Adsorption in binary component systems

3.3.1. Adsorption equilibrium isotherms

The Langmuir and Freundlich isotherm models were adopted to fit the experimental data and are shown in Fig. 11. Besides, the parameters calculated from the equations of the Langmuir and Freundlich isotherm models are listed in Table 5. It is can be seen from Fig. 11 that both the two models fitted the data well, while the Langmuir model fitted better compared to the Freundlich model for the higher R^2 ($R^2 > 0.99$) of the first one (Table 5), similar to the single component systems. In comparison with the single component systems, it is clear that the maximum adsorption capacities of BV and BG decreased from 90.1765 to 41.8557 mg/g and 99.7308 to 43.8446 mg/g, respectively, which suggested that competitive adsorption occurred in the aqueous solution mixture between the two cationic dyes.

Since BV and BG are the same-type dyes, they would compete with each other for the active adsorption sites of the adsorbent whose quantity is finite in the solution mixture. It is a common phenomenon that the maximum adsorption capacities of each component in the mixture systems are smaller than those of the single component systems, but the degrees of decline may differ with the diverse kinds of dyes [65]. In addition, the adsorption capacity of BG appeared to be higher than that of BV in the cationic binary component system (Fig. 12), which could be attributed to the different competitive abilities for adsorption and further might be relevant to the distinctions of structures and sizes of the dye molecules [66]. It was easier for BG molecules to diffuse into inner pores of the adsorbent because of their smaller sizes, making it more dominant than BV in the binary component systems [61].

Table 4
Thermodynamic parameters for adsorption of BV and BG onto MCM-4 at various temperatures in single component systems

Dyes	C_0	ΔH°	ΔS°	ΔG°		
				25℃	30℃	40℃
BV	100	−15.161	−35.179	−4.663	−4.525	−4.142
	150	−5.926.	−6.692	−3.931	−3.901	−3.831
	200	−4.203	−3.091	−3.296	−3.195	−3.244
BG	100	−32.118	−84.048	−7.148	−6.264	−5.782
	150	−21.542	−51.911	−5.954	−5.730	−5.551
	200	−10.678	−19.658	−4.845	−4.703	−4.515

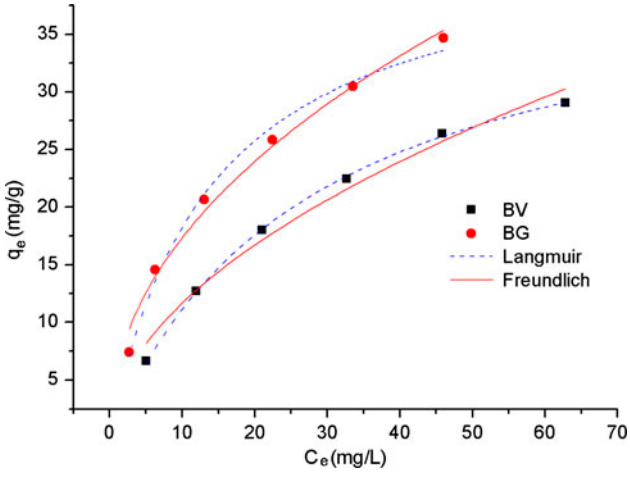

Fig. 11. Adsorption equilibrium isotherms of BV and BG onto MCM-41 in binary component systems (Conditions: pH 5.0, 25℃, MCM-41 dosage 0.3 g).

3.3.2. Adsorption kinetics

Fig. 13 presents the kinetic adsorption profiles of BV and BG onto MCM-41 in the binary component system with the same initial dye concentration at different time. As seen from Fig. 13, the removal percentages of both BV and BG dye molecules increased with time, until adsorption equilibrium was reached in the end. However, both the removal ratios were smaller in the binary-dye systems compared to the single systems, which was in consistent with the results of the adsorption equilibrium isotherm study of BV and BG onto MCM-41 in single component systems. In addition, the extent of the removal ratio of BV was higher than that of BG in the binary system, which confirmed the existence of competition between the two dyes in the binary-dye systems [67]. Besides, two connatural cationic dyes were mixed in the aqueous solution at the same concentrations, leading to the concentration of each dye was half of that of the single component systems in reality. And the adsorption capacity of dye would increase with the initial dye concentration, which could also cause the drop of the adsorption capacity of each dye [68].

Four kinetic models (the pseudo-first-order, pseudo-second-order, Spahn and Schlunder, and intra-particle diffusion models) were applied to fit the experiments and the kinetic results were illustrated in Fig. 13 and Table 6. It was seen from Table 6 that the

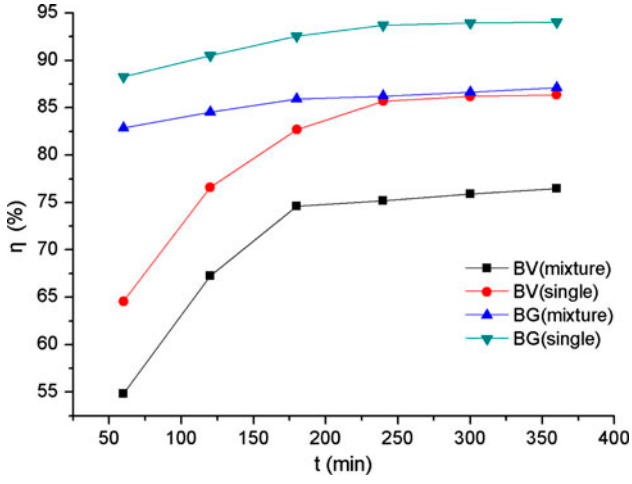

Fig. 12. Effect of contact time on adsorption of the two cationic dyes in binary component systems (Conditions: pH 5.0, 25℃, MCM-41 dosage 0.3 g, dye concentration 100 mg/L).

Table 5
Adsorption isotherm constants for adsorption of BV and BG onto MCM-41 at various temperatures in binary component systems

Dyes	Temperature (℃)	Langmuir			Freundlich		
		q_m	K_L	R^2	K_F	n	R^2
BV	25	41.8557	0.0362	0.9994	3.5327	1.9273	0.9796
BG	25	43.8446	0.0713	0.9904	5.9302	2.1447	0.9849

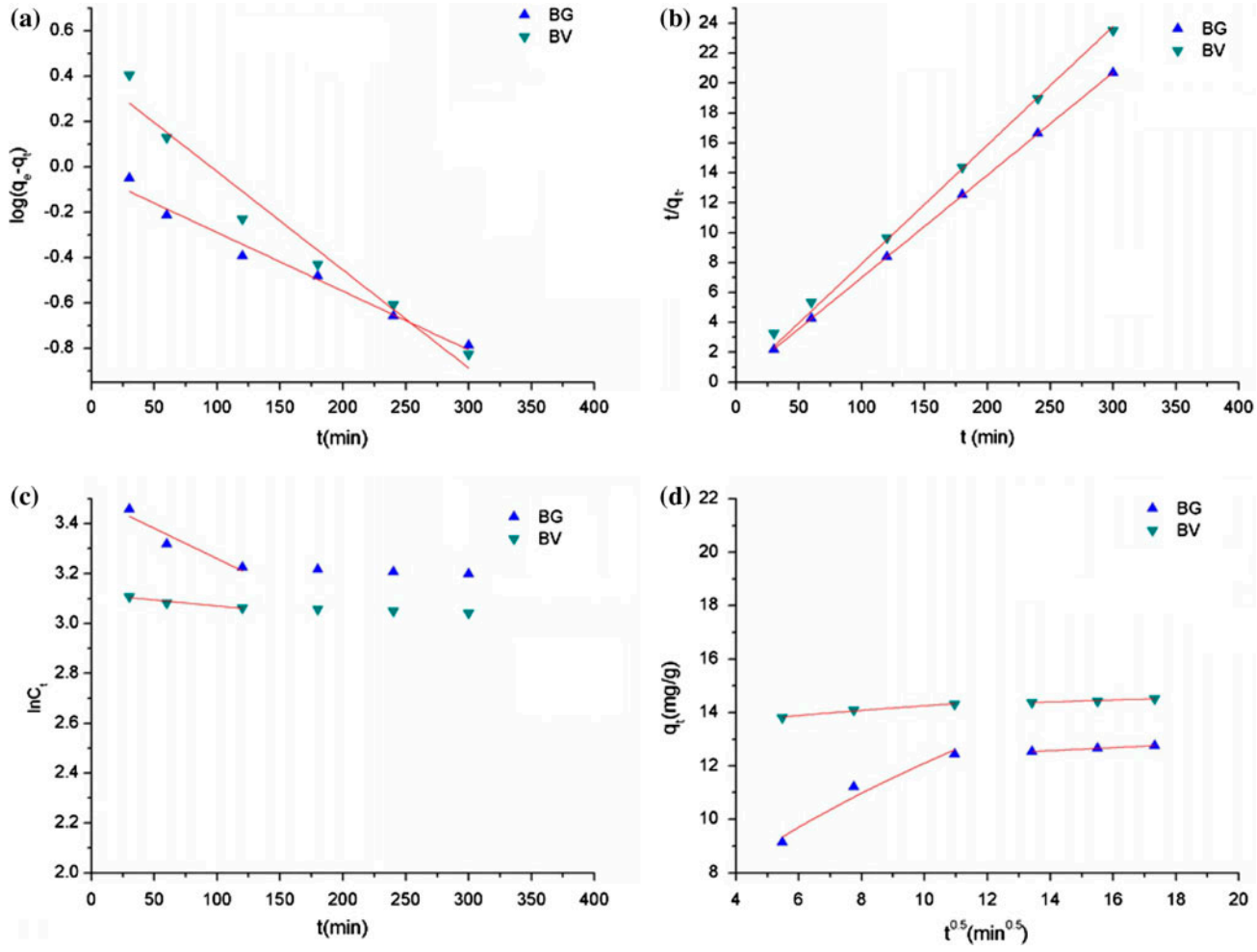

Fig. 13. Adsorption kinetics of BV and BG onto MCM-41 in binary component systems. (a) Pseudo-first-order kinetic model fitting, (b) Pseudo-second-order kinetic model fitting, (c) Spahn and Schlunder model fitting, and (d) Intraparticle diffusion model fitting (Conditions: pH 5.0, 25°C, MCM-41 dosage 0.3 g).

adsorption followed the pseudo-second-order model better in comparison with the pseudo-first-order model since the R^2 value of the former ($R^2 > 0.994$) was higher than that of the latter ($R^2 > 0.950$), in accordance to the kinetic results of the single component systems, which also indicated that the cationic dye adsorption onto the adsorbent MCM-41 would be altered in the binary component systems [66]. From Fig. 13(c) we can know that the relationships between ln C_t and t of the two cationic dyes were linear, suggesting the great influence of the out-diffusion from the liquid to MCM-41 surface of the entire adsorption process in the binary component systems. Fig. 13(d) presented two straight lines after the intraparticle diffusion kinetic fitting, demonstrating that there existed at least two processes controlling the adsorption rate in the mixed systems.

Comparing the parameters summarized in Tables 3 and 6, the values of $k_{p,2}$ in the binary component systems became smaller than those of the previous single systems (Binary: 4.1474 (BV), 1.4729 (BG); Single: 3.3662 (BV), 0.5154 (BG)). Whereas the $k_{p,3}$ value of BG increased from 0.2087 to 0.2906, simultaneously it just decreased slightly for BV, which might be attributed to the synthetical effects of the competitive adsorption and the concentration of the dyes in the mixed aqueous solution.

3.4. Desorption study

Desorption and regeneration of the adsorbent is quite a vital characteristic which can lower the cost of adsorbents in practical applications effectually. Fig. 14

Table 6
Kinetic parameters for adsorption of BV and BG onto MCM-41 in binary component systems

	Pseudo-first-order kinetic model			Pseudo-second-order kinetic model			Spahn and schlunder model		Intraparticle diffusion model			
Dyes	k_1	q_e	R^2	k_2	q_e	R^2	k_{ext}	R^2	$k_{p,2}$	R^2	$k_{p,3}$	R^2
BV	0.0100	1.5091	0.9546	0.0514	12.6087	0.9949	0.0024	0.8193	3.3662	0.9238	0.4455	0.9997
BG	0.0060	0.9699	0.9755	0.0322	14.5877	0.9999	0.0005	0.8864	0.5154	0.9772	0.2906	0.9698

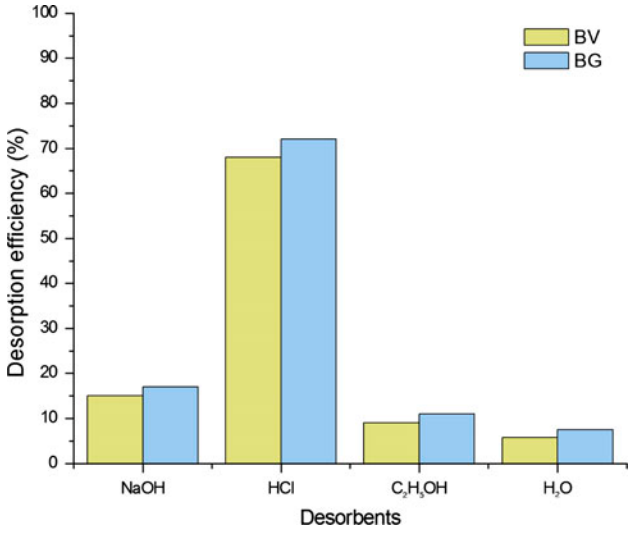

Fig. 14. Desorption efficiency of BV and BG released by saturated MCM-41 after treatment processes with three different kinds of desorbents (0.1 M NaOH, 0.1 M HCl, and 10% C_2H_5OH solutions) in the batch tests.

presents the desorption efficiency of BV and BG released by saturated MCM-41 after treatment processes with three different kinds of desorbents.

As seen from Fig. 14, it could be inferred that solution pH had a great influence on the desorption process. In NaOH aqueous solution, since MCM-41 surface is electronegative, the cationic dye molecules are difficult to be displaced due to the electrostatic repulsion. However, the binding affinity of hydrogen ion for the negative-charged MCM-41 is higher than that of cationic dyes BV and BG, which makes the ion exchange reactions occur easier between H^+ and cationic dye molecules on MCM-41 surface [68]. In addition, electrostatic interaction is also a dominant mechanism of desorption process in the acid environment.

4. Conclusion

The performance of MCM-41 of removing two cationic dyes (BV and BG) from aqueous solutions has been investigated in this work. In single systems, maximum monolayer removal percentage by this adsorbent is 86.81% for dye BV and 94.97% for dye BG at pH 5.0 and 25°C. In addition, it was observed that both the removal percentages of BV and BG by MCM-41 increased with the adsorbent dosage and contact time, but decreased with the initial dye concentration and temperature of the system. The equilibrium data agreed very well with Langmuir isotherm model, and E values resulted from the D–R isotherm fitting were all less than 8 kJ/mol, indicating the adsorption to be monolayer and physical in nature. The adsorption kinetics were best fitted by the Lagergren pseudo-second-order model, and both the external diffusion and intraparticle diffusion were rate-controlling steps. The values of the thermodynamic functions suggested that the adsorption process was feasible, spontaneous, and exothermic. What is more, competitive adsorption between the two cationic dyes existed in binary component systems, which might result in that the adsorption capacity and removal percentage of the binary system were lower than those of the single systems. The adsorption isotherm and kinetic data of the binary component systems could also be well correlated by the Langmuir model and Lagergren pseudo-second order model, respectively. High desorption and regeneration efficiency of BV and BG from saturated MCM-41 by NaOH solution also shows that MCM-41 can be well applied for cationic dyes removal from industrial wastewater.

Acknowledgements

The authors are thankful for the financial support by the Priority Academic Program Development of Jiangsu Higher Education Institution.

Symbols

C_e — liquid phase dye concentration at equilibrium (mg/L)
C_0 — initial liquid concentrations of dye (mg/L)
C_2 — liquid dye concentration after desorption equilibrium (mg/L)
C_t — liquid concentrations of dye at any time (mg/L)
C_{ad} — liquid concentrations of reduced dye (mg/L)
C — a constant related to the boundary layer
k_1 — equilibrium rate constant of pseudo-first-order adsorption (/min)
k_2 — equilibrium rate constant of pseudo-second-order adsorption (g/(mg min))
k_{ext} — external diffusion constant (/min)
$k_{p,i}$ — the intraparticle diffusion rate parameters of different stages
K — the constant giving the mean free energy of adsorption per molecular of the adsorbate
K_0 — the equilibrium constant
K_F — Freundlich constant indicative of the relative adsorption capacity of the sorbent (mg/g)
K_L — Langmuir sorption constant (L/mg)
K_T — empirical Temkin constant related to the equilibrium binding constant (L/mg)
q_e — amount of solute adsorbed per unit weight of the adsorbent at equilibrium (mg/g)
q_m — monolayer maximum sorption capacity of the adsorbent (mg/g)
q_t — amount of solute adsorbed per unit weight of the adsorbent at any time (mg/g)
b — Temkin constant related to the heat of adsorption (kJ/mol)
R — gas constant (8.314 J/(mol K))
R^2 — correlation coefficient
E — mean free energy of sorption (kJ/mol)
T — absolute temperature (°C)
T — time (min)
M — weight of the dyes used (g)
V — volume of the aqueous solution (L)
V_1 — volume of aqueous solution for the adsorption reaction (L)
V_2 — volume of aqueous solution for the desorption reaction (L)
α — initial adsorption rate (mol/(g min))
β — desorption constant (g/mol)
η — adsorptive removal efficiency of the dye
γ — dye desorption efficiency
ε — Polanyi potential
n — Freundlich constant indicative of the intensity of adsorption

References

[1] L. Torkian, B.G. Ashtiani, E. Amereh, N. Mohammadi, Adsorption of Congo red onto mesoporous carbon material: Equilibrium and kinetic studies, Desalin. Water Treat. 44 (2012) 118–127.
[2] S.S. Bayazit, Investigation of Safranin O adsorption on superparamagnetic iron oxide nanoparticles (SPION) and multi-wall carbon nanotube/SPION composites, Desalin. Water Treat. 52 (2014) 6966–6975.
[3] Z. Liu, Y. Liu, L. Chen, H. Zhang, Performance study of heavy metal ion adsorption onto microwave-activated banana peel, Desalin. Water Treat. 52 (2014) 7117–7124.
[4] B.A. Fil, C. Özmetin, Adsorption of cationic dye from aqueous solution by clay as an adsorbent: Thermodynamic and kinetic studies, J. Chem. Soc. Pak. 34 (2012) 896–906.
[5] G.O. El-Sayed, Removal of methylene blue and crystal violet from aqueous solutions by palm kernel fiber, Desalination 272 (2011) 225–232.
[6] J.L. Figueiredo, J.P.S. Sousa, C.A. Orge, M.F.R. Pereira, J.J.M. Órfão, Adsorption of dyes on carbon xerogels and templated carbons: Influence of surface chemistry, Adsorption 17 (2011) 431–441.
[7] M. Korkmaz, C. Özmetin, B.A. Fil, E. Özmetin, Y. Yasar, Methyl Violet dye adsorption onto clinoptilolite (Natural Zeolite): Isotherm and kinetic study, Fresen. Environ. Bull. 22 (2013) 1524–1533.
[8] M. Visa, L. Andronic, D. Lucaci, A. Duta, Concurrent dyes adsorption and photo-degradation on fly ash based substrates, Adsorption 17 (2011) 101–108.
[9] L. Zhang, H. Zhang, W. Guo, Y. Tian, Removal of malachite green and crystal violet cationic dyes from aqueous solution using activated sintering process red mud, Appl. Clay Sci. 93–94 (2014) 85–93.
[10] E. Aladağ, B.A. Fil, R. Boncukcuoğlu, O. Sözüdoğru, A.E. Yılmaz, Adsorption of Methyl Violet Dye, a textile industry effluent onto montmorillonite—Batch study, J. Dispersion Sci. Technol. 35 (2014) 1737–1744.
[11] A.K. Kushwaha, N. Gupta, M. Chattopadhyaya, Enhanced adsorption of methylene blue on modified silica gel: Equilibrium, kinetic, and thermodynamic studies, Desalin. Water Treat. 52 (2014) 4527–4537.
[12] E. Kalkan, H. Nadaroğlu, N. Celebi, G. Tozsin, Removal of textile dye Reactive Black 5 from aqueous solution by adsorption on laccase-modified silica fume, Desalin. Water Treat. 52 (2014) 6122–6134.
[13] G. Asgari, B. Ramavandi, S. Sahebi, Removal of a cationic dye from wastewater during purification by Phoenix dactylifera, Desalin. Water Treat. 52 (2014) 7354–7365.
[14] B. Fil, M. Yilmaz, S. Bayar, M. Elkoca, Investigation of adsorption of the dyestuff astrazon Red Violet 3rn (Basic Violet 16) on montmorillonite clay, Braz. J. Chem. Eng. 31 (2014) 171–182.
[15] M. Mohammad, S. Maitra, N. Ahmad, A. Bustam, T. Sen, B.K. Dutta, Metal ion removal from aqueous solution using physic seed hull, J. Hazard. Mater. 179 (2010) 363–372.
[16] F. Ba, Y. Ae, Removal of cationic dye (Basic Red 18) from aqueous solution using natural Turkish clay, Global Nest J. 15 (2013) 529–541.

[17] E. Forgacs, T. Cserháti, G. Oros, Removal of synthetic dyes from wastewaters: A review, Environ. Int. 30 (2004) 953–971.
[18] Y.C. Sharma, Optimization of parameters for adsorption of methylene blue on a low-cost activated carbon, J. Chem. Eng. Data 55 (2009) 435–439.
[19] M.A. Ahmad, R. Alrozi, Removal of malachite green dye from aqueous solution using rambutan peel-based activated carbon: Equilibrium, kinetic and thermodynamic studies, Chem. Eng. J. 171 (2011) 510–516.
[20] S. Dawood, T.K. Sen, Removal of anionic dye Congo red from aqueous solution by raw pine and acid-treated pine cone powder as adsorbent: Equilibrium, thermodynamic, kinetics, mechanism and process design, Water Res. 46 (2012) 1933–1946.
[21] P. Selvam, S.K. Bhatia, C.G. Sonwane, Recent advances in processing and characterization of periodic mesoporous MCM-41 silicate molecular sieves, Ind. Eng. Chem. Res. 40 (2001) 3237–3261.
[22] L.C. Juang, C.C. Wang, C.K. Lee, Adsorption of basic dyes onto MCM-41, Chemosphere 64 (2006) 1920–1928.
[23] S. Koner, A. Pal, A. Adak, Cationic surfactant adsorption on silica gel and its application for wastewater treatment, Desalin. Water Treat. 22 (2010) 1–8.
[24] J.S. Beck, J.C. Vartuli, W.J. Roth, M.E. Leonowicz, C.T. Kresge, K.D. Schmitt, C.T.W. Chu, D.H. Olson, E.W. Sheppard, A new family of mesoporous molecular sieves prepared with liquid crystal templates, J. Am. Chem. Soc. 114 (1992) 10834–10843.
[25] M. Paul, N. Pal, A. Bhaumik, Selective adsorption and release of cationic organic dye molecules on mesoporous borosilicates, Mater. Sci. Eng. C 32 (2012) 1461–1468.
[26] J. Choma, M. Jaroniec, W. Burakiewicz-Mortka, M. Kloske, Critical appraisal of classical methods for determination of mesopore size distributions of MCM-41 materials, Appl. Surf. Sci. 196 (2002) 216–223.
[27] J. Wloch, M. Rozwadowski, M. Lezanska, K. Erdmann, Analysis of the pore structure of the MCM-41 materials, Appl. Surf. Sci. 191 (2002) 368–374.
[28] S.A. El-Safty, Functionalized hexagonal mesoporous silica monoliths with hydrophobic azo-chromophore for enhanced Co(II) ion monitoring, Adsorption 15 (2009) 227–239.
[29] B. Noroozi, G. Sorial, H. Bahrami, M. Arami, Adsorption of binary mixtures of cationic dyes, Dyes Pigm. 76 (2008) 784–791.
[30] C. Kresge, M. Leonowicz, W. Roth, J. Vartuli, J. Beck, Ordered mesoporous molecular sieves synthesized by a liquid-crystal template mechanism, Nature 359 (1992) 710–712.
[31] A.B. Ardakani, H. Panahi, A. Hasani, A. Javid, E. Moniri, Tin(IV) oxide nanoparticles grafted with N, N-dimethylacrylamide–allyl butyl ether for xylene adsorption, Int. J. Environ. Sci. Technol. 12 (2015) 1613–1624.
[32] A. Heidari, H. Younesi, Z. Mehraban, Removal of Ni (II), Cd(II), and Pb(II) from a ternary aqueous solution by amino functionalized mesoporous and nano mesoporous silica, Chem. Eng. J. 153 (2009) 70–79.
[33] D.O. Santos, M. de Lourdes Nascimento Santos, J.A.S. Costa, R.A. de Jesus, S. Navickiene, E.M. Sussuchi, M.E. de Mesquita, Investigating the potential of functionalized MCM-41 on adsorption of Remazol Red dye, Environ. Sci. Pollut. Res. 20 (2013) 5028–5035.
[34] Z. Chen, L. Zhou, F. Zhang, C. Yu, Z. Wei, Multicarboxylic hyperbranched polyglycerol modified SBA-15 for the adsorption of cationic dyes and copper ions from aqueous media, Appl. Surf. Sci. 258 (2012) 5291–5298.
[35] L. Tian, G. Xie, R. Li, X. Yu, Y. Hou, Removal of Cr (VI) from aqueous solution using MCM-41, Desalin. Water Treat. 36 (2011) 334–343.
[36] V.P. Vinod, T.S. Anirudhan, Adsorption behaviour of basic dyes on the humic acid immobilized pillared clay, Water Air Soil Pollut. 150 (2003) 193–217.
[37] Y. Wu, M. Zhang, H. Zhao, S. Yang, A. Arkin, Functionalized mesoporous silica material and anionic dye adsorption: MCM-41 incorporated with amine groups for competitive adsorption of acid fuchsine and acid orange II, RSC Adv. 4 (2014) 61256–61267.
[38] G. Crini, Non-conventional low-cost adsorbents for dye removal: A review, Bioresour. Technol. 97 (2006) 1061–1085.
[39] V. Vadivelan, K.V. Kumar, Equilibrium, kinetics, mechanism, and process design for the sorption of methylene blue onto rice husk, J. Colloid Interface Sci. 286 (2005) 90–100.
[40] P. Senthil Kumar, S. Ramalingam, C. Senthamarai, M. Niranjanaa, P. Vijayalakshmi, S. Sivanesan, Adsorption of dye from aqueous solution by cashew nut shell: Studies on equilibrium isotherm, kinetics and thermodynamics of interactions, Desalination 261 (2010) 52–60.
[41] Q. Qin, Selective Adsorption of Pollutants by Functionalized Mesoporous Molecular Sieves MCM-41 from Aqueous Solution, Published PhD dissertation, Harbin Institute of Technology, 2009.
[42] M. Anbia, S. Salehi, Removal of acid dyes from aqueous media by adsorption onto amino-functionalized nanoporous silica SBA-3, Dyes Pigm. 94 (2012) 1–9.
[43] A. Khataee, G. Dehghan, A. Ebadi, M. Zarei, M. Pourhassan, Biological treatment of a dye solution by *Macroalgae Chara* sp.: Effect of operational parameters, intermediates identification and artificial neural network modeling, Bioresour. Technol. 101 (2010) 2252–2258.
[44] A. Olgun, N. Atar, Removal of copper and cobalt from aqueous solution onto waste containing boron impurity, Chem. Eng. J. 167 (2011) 140–147.
[45] M.A.M. Salleh, D.K. Mahmoud, W.A.W.A. Karim, A. Idris, Cationic and anionic dye adsorption by agricultural solid wastes: A comprehensive review, Desalination 280 (2011) 1–13.
[46] M. Ghaedi, J. Tashkhourian, A.A. Pebdani, B. Sadeghian, F.N. Ana, Equilibrium, kinetic and thermodynamic study of removal of reactive orange 12 on platinum nanoparticle loaded on activated carbon as novel adsorbent, Korean J. Chem. Eng. 28 (2011) 2255–2261.
[47] X. Peng, D. Huang, T. Odoom-Wubah, D. Fu, J. Huang, Q. Qin, Adsorption of anionic and cationic dyes on ferromagnetic ordered mesoporous carbon from aqueous solution: Equilibrium, thermodynamic and kinetics, J. Colloid Interface Sci. 430 (2014) 272–282.

[48] Y. Wu, J. Cao, P. Yilihan, Y. Jin, Y. Wen, J. Zhou, Adsorption of anionic and cationic dyes from single and binary systems by industrial waste lead–zinc mine tailings, RSC Adv. 3 (2013) 10745–10753.
[49] X. Li, G. Wang, W. Li, P. Wang, C. Su, Adsorption of acid and basic dyes by sludge-based activated carbon: Isotherm and kinetic studies, J. Cent. South Univ. 22 (2015) 103–113.
[50] P. Monash, G. Pugazhenthi, Adsorption of crystal violet dye from aqueous solution using mesoporous materials synthesized at room temperature, Adsorption 15 (2009) 390–405.
[51] Ö. Demirbaş, Y. Turhan, M. Alkan, Thermodynamics and kinetics of adsorption of a cationic dye onto sepiolite, Desalin. Water Treat. 54 (2014) 707–714.
[52] H. Spahn, E. Schlünder, The scale-up of activated carbon columns for water purification, based on results from batch tests—I: Theoretical and experimental determination of adsorption rates of single organic solutes in batch tests, Chem. Eng. Sci. 30 (1975) 529–537.
[53] W. Fritz, W. Merk, E. Schlünder, Competitative adsorption of two dissolved organics onto activated carbon—II: Adsorption kinetics in batch reactors, Chem. Eng. Sci. 36 (1981) 743–757.
[54] P. Luo, Y. Zhao, B. Zhang, J. Liu, Y. Yang, J. Liu, Study on the adsorption of Neutral Red from aqueous solution onto halloysite nanotubes, Water Res. 44 (2010) 1489–1497.
[55] M. Kousha, E. Daneshvar, H. Dopeikar, D. Taghavi, A. Bhatnagar, Box–Behnken design optimization of Acid Black 1 dye biosorption by different brown macroalgae, Chem. Eng. J. 179 (2012) 158–168.
[56] F.C. Wu, R.L. Tseng, R.S. Juang, Comparisons of porous and adsorption properties of carbons activated by steam and KOH, J. Colloid Interface Sci. 283 (2005) 49–56.
[57] D. Ranjan, M. Talat, S. Hasan, Biosorption of arsenic from aqueous solution using agricultural residue 'rice polish', J. Hazard. Mater. 166 (2009) 1050–1059.
[58] L. Ai, J. Jiang, Removal of methylene blue from aqueous solution with self-assembled cylindrical graphene–carbon nanotube hybrid, Chem. Eng. J. 192 (2012) 156–163.
[59] W. Konicki, K. Cendrowski, X. Chen, E. Mijowska, Application of hollow mesoporous carbon nanospheres as an high effective adsorbent for the fast removal of acid dyes from aqueous solutions, Chem. Eng. J. 228 (2013) 824–833.
[60] N. Graham, X. Chen, S. Jayaseelan, The potential application of activated carbon from sewage sludge to organicdyes removal, Water Sci. Technol. 43 (2001) 245–252.
[61] S. Wang, H. Li, L. Xu, Application of zeolite MCM-22 for basic dye removal from wastewater, J. Colloid Interface Sci. 295 (2006) 71–78.
[62] F. Krika, O.e.F. Benlahbib, Removal of methyl orange from aqueous solution via adsorption on cork as a natural and low-coast adsorbent: Equilibrium, kinetic and thermodynamic study of removal process, Desalin. Water Treat. 53(2015) 3711–3723.
[63] A.M. Aljeboree, A.F. Alkaim, A.H. Al-Dujaili, Adsorption isotherm, kinetic modeling and thermodynamics of crystal violet dye on coconut husk-based activated carbon, Desalin. Water Treat. 53 (2015) 3656–3667.
[64] A. Rodríguez, J. García, G. Ovejero, M. Mestanza, Adsorption of anionic and cationic dyes on activated carbon from aqueous solutions: Equilibrium and kinetics, J. Hazard. Mater. 172 (2009) 1311–1320.
[65] Y. Al-Degs, M. Khraisheh, S. Allen, M. Ahmad, G. Walker, Competitive adsorption of reactive dyes from solution: Equilibrium isotherm studies in single and multisolute systems, Chem. Eng. J. 128 (2007) 163–167.
[66] Y. Wu, L. Jiang, Y. Wen, J. Zhou, S. Feng, Biosorption of Basic Violet 5BN and Basic Green by waste brewery's yeast from single and multicomponent systems, Environ. Sci. Pollut. Res. 19 (2012) 510–521.
[67] R. Saad, S. Hamoudi, K. Belkacemi, Adsorption of phosphate and nitrate anions on ammonium-functionnalized mesoporous silicas, J. Porous Mater. 15 (2008) 315–323.
[68] S. Eftekhari, A. Habibi-Yangjeh, S. Sohrabnezhad, Application of AlMCM-41 for competitive adsorption of methylene blue and rhodamine B: Thermodynamic and kinetic studies, J. Hazard. Mater. 178 (2010) 349–355.